

## **Chapter Three: Guest/Host Relationships using Chiral Imidazolium Structure Directing Agents in Molecular Sieve Synthesis**

### **3.1: Introduction**

The results presented in Chapter Two showed 42 instances of Beta across seven imidazolium SDA. Beta was favored as the SDAs became larger with bis(cyclooctyl) SDA **13** only making Beta. This apparent strong specificity for Beta lead to an additional guest/host study using chiral imidazolium SDAs.

Zeolite Beta was discovered in the 1960s by workers at Mobil using tetraethylammonium hydroxide as SDA<sup>1</sup>. Indirect characterization methods using probe molecule adsorption and catalytic testing suggested a large pore multi-dimensional structure. The exact structure remained unknown until the late 1980s when it was independently solved by workers at Exxon<sup>2, 3</sup> and Mobil<sup>4</sup>. The proposed structure is an intergrowth of two pure end-members denoted polymorphs A and B. Lateral shifts along a and b between adjacent layers determine the structure. The basic Beta layer is shown in Figure 3.1 together with representations for three ordered polymorphs. Details of the possible stacking sequences leading to the various end members are available online from the Database of Zeolite Structures<sup>5</sup>.

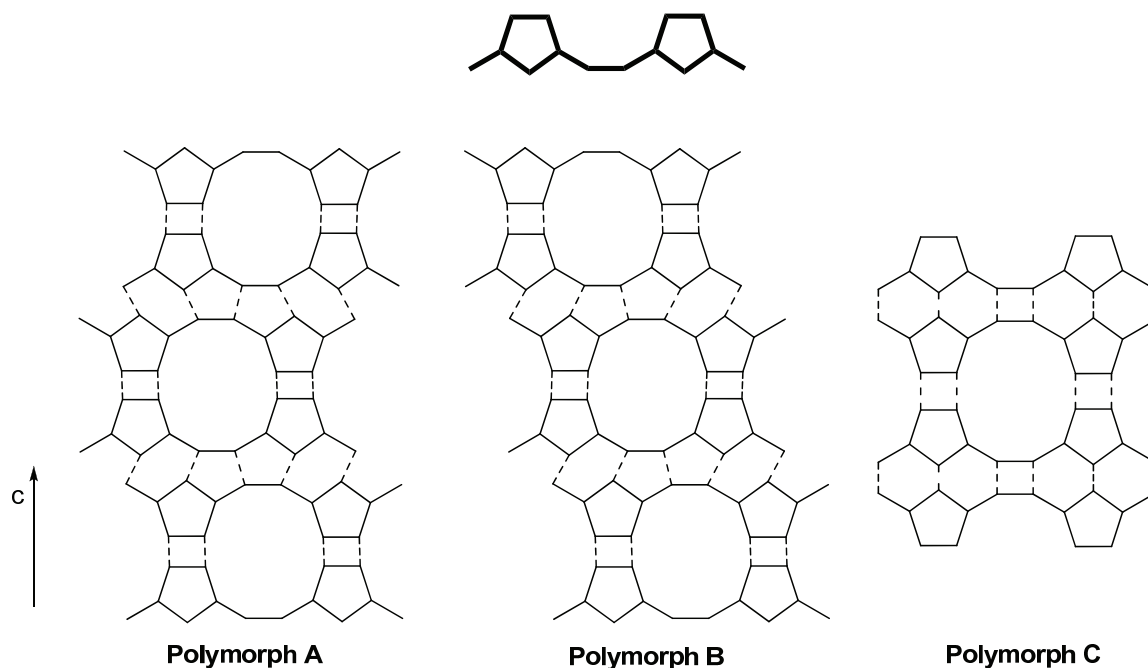


Figure 3.1: Beta building layer and representations of Polymorphs A, B and C. For clarity oxygen atoms have been omitted. Solid lines connect neighboring silicon atoms in each layer unit and dashed lines connect silicon atoms in adjacent layers

Tetragonal polymorph A contains two enantiomorphs with  $P4_122$  or  $P4_322$  symmetry. Monoclinic polymorph B is achiral with symmetry  $C2/c$  (often lowered to  $P(-1)$  for comparison with other polymorphs). Traditional Beta products are achiral with equal amounts of “right-” and “left-handed” polymorph A intergrown with polymorph B. The possibility of synthesizing a chiral Beta material has been actively pursued by many groups since publication of the structure. Potential applications of an enantiopure zeolite could include chiral catalysis and separations. Examples of chiral frameworks in compositions other than high-silica exist and have been recently discussed<sup>6</sup>. Many of the reported materials are phosphate-based with reduced hydrothermal stability. Two recent reports of

chiral germanosilicates SU-32 (P<sub>6</sub><sub>1</sub>22/P<sub>6</sub><sub>5</sub>22)<sup>7</sup> and ITQ-37 (P<sub>4</sub><sub>1</sub>32/P<sub>4</sub><sub>3</sub>32)<sup>8</sup> also noted limited hydrothermal stability compared to high-silica molecular sieves. Neither material employed chiral organic molecules in their synthesis.

Additional polymorphs were predicted from the \*BEA layer elucidated in the aforementioned references. One stacking sequence (0a, 0b) forms a structure rich in double four rings (D4R, a cube) and is denoted polymorph C<sup>2</sup>. This subunit appears frequently in germanosilicate materials with Ge preferentially occupying sites in the D4R<sup>9</sup> subunits. Beta polymorph C (BEC) was synthesized as a pure germanium dioxide material (FOS-5)<sup>10</sup> and germanosilicate (ITQ-17)<sup>11</sup>. Recently, germanium free ITQ-17 has been synthesized using Diels-Alder derived SDAs<sup>12, 13</sup>. The germanium free syntheses required fluoride to stabilize the D4R subunits. Another stacking sequence forms an ordered intergrowth of polymorphs A and B that is denoted polymorph C<sub>H</sub> (polymorph C-Higgins)<sup>4</sup>. A material denoted SSZ-63<sup>14</sup> exhibits X-ray diffraction (XRD) reflections more closely resembling Polymorph C<sub>H</sub> than those expected for typical Beta (random polymorph A/B intergrowth).

Structural differences brought about by different stacking sequences manifest in changes to XRD patterns. Diffraction patterns for faulted materials can be simulated using software programs such as DIFFaX<sup>15</sup>. Simulated diffraction patterns can be generated for a series of fault probabilities that can be compared to experimental patterns. The relative contribution of polymorphs A and B to Beta was estimated using this process. This also provides a valuable tool for this study as experimental XRD patterns can be compared to those expected for increasing polymorph A content. Figure 3.2 presents simulated XRD patterns for polymorphs A and B. In the context of enriched polymorph A two features should appear in the XRD pattern. The first is separation of the broad, almost symmetrical

reflection between 7 and 8°2 $\theta$  into two resolved reflections with appropriate intensity. The second feature is the appearance of a reflection at  $\sim 9.7^\circ 2\theta$  with increasing polymorph A content. This second feature does not overlap with any reflections from polymorph B making it valuable in assessing polymorph A enrichment.

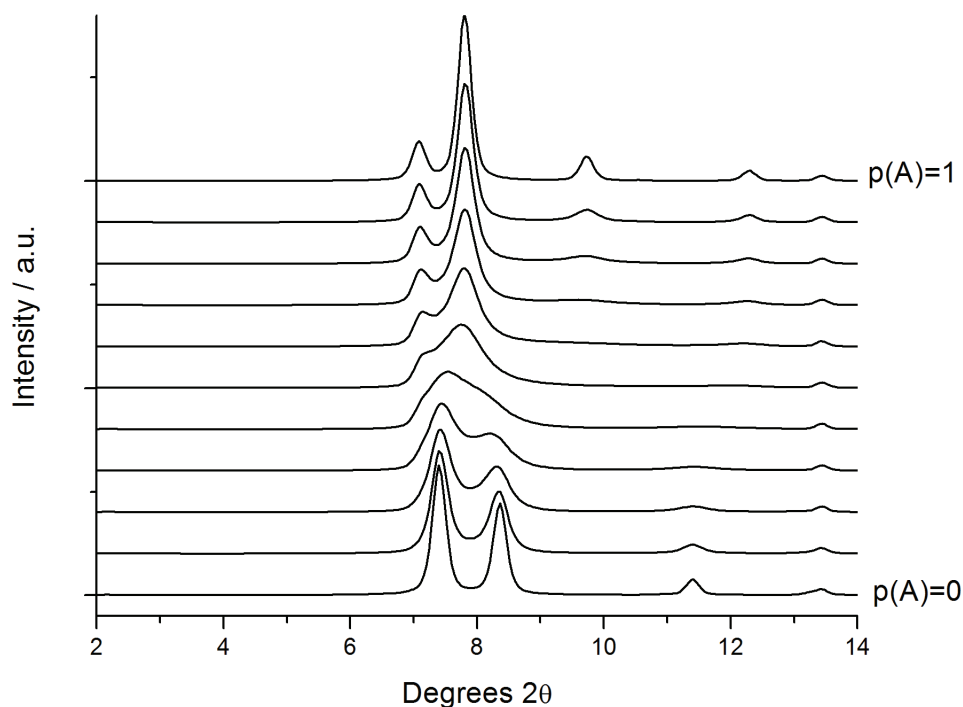


Figure 3.2: Simulated XRD patterns for Beta polymorphs A and B. Bottom to top=100% polymorph B ( $p(A)=0$ ) to 100% polymorph A ( $p(A)=1$ ))

In the wider context of rational design of molecular sieves, Davis and Lobo proposed several criteria considered necessary to synthesize pure polymorph A<sup>16</sup>. The proposed criteria envisioned the use of a true template molecule. A hypothetical template/chiral zeolite composite would have lower energy compared to all other silicate

structures. Therefore, this molecule would strictly specify the formation of Polymorph A. Additional constraints were as follows:

- (i) The molecule must be chiral.
- (ii) The molecule must be  $> 10\text{\AA}$  in length.
- (iii) The molecule must be stable under synthesis conditions.

Previous studies with imidazoliums have not shown any true templates although several show strong specificity to a given product. Therefore, exploring chiral imidazolium SDAs might offer a chance to synthesize enriched polymorph A. Chiral imidazolium salts have been synthesized as precursors to chiral N-heterocyclic carbene (NHC) ligands in organometallic complexes<sup>17–20</sup>. NHC compounds have also been applied in asymmetric organocatalysis<sup>21, 22</sup>. The synthetic methods for these  $C_2$ -symmetric imidazoliums are identical to those used in Chapter Two with chiral primary amines the chiral source. Figure 3.3 shows the chiral imidazolium SDAs used in the present study. The chiral SDA library covers a similar  $C/N^+$  range to the SDAs found to make Beta in Chapter Two. Four of the five SDAs contain a chiral carbon adjacent to nitrogen, whereas the remaining one derives chirality from the pinene-precursor. Although the ability to direct a specific product is not known *a priori*, all five were expected to meet the additional constraints listed above.

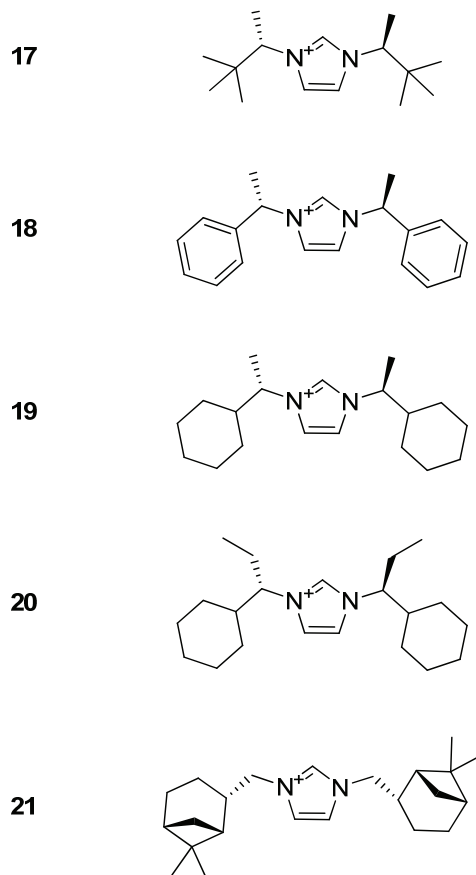
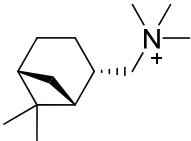
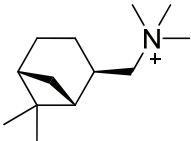
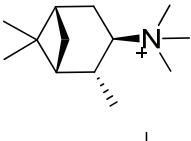
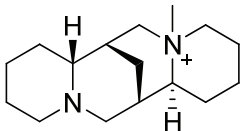
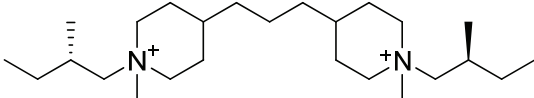
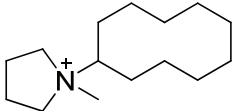
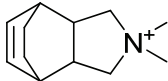
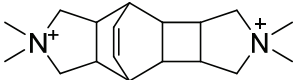


Figure 3.3: Chiral imidazolium SDAs studied

Selected examples of chiral SDAs reported in molecular sieve synthesis are given in Table 3.1. Also included in Table 3.1 are three SDAs that have given Beta products enriched in certain Polymorphs. SDAs **I-III** derive chirality from the pinene skeleton and all three produce achiral products. Additional pinene-derived SDAs were investigated with MTW the only additional phase<sup>23</sup>. (-)-sparteine derived SDA **IV** has been used to synthesize four high-silica phases. In all cases the product phases are achiral. Other sparteine-derived SDAs have been investigated with CFI the only phase obtained<sup>24, 25</sup>. SDA **V** was reported to synthesize MTW+Beta with this the only apparent report of a

chiral organocation synthesizing any Beta material. It should be noted that a report of slight polymorph A enrichment has appeared, although no details of the organic were reported<sup>16</sup>.

Table 3.1: Examples of chiral SDAs used in molecular sieve synthesis and SDAs used to synthesize enriched Beta products

SDA	Structure	Product	Reference
I		CIT-1 (CON)	26
II		CIT-1 (CON)	26
III		SSZ-31 (*STO)	26
IV		SSZ-24 (AFI), CIT-5 (CFI), ITQ-21, ITQ-30	27–30
V		ZSM-12 (MTW)+Beta	31
VI		SSZ-63 (enriched Polymorph C <sub>H</sub> )	14
VII		Pure-silica Beta C, enriched Polymorph B	12, 32
VIII		Pure-silica Beta C	13

The three remaining SDA give Beta products enriched in various polymorphs. Both **VII** and **VIII** require fluoride to synthesize pure-silica BEC using the cooperative effect of fluoride stabilized D4Rs. Reactions using **VII** also required KOH with  $K_2SiF_6$  buffering deemed necessary to form BEC. The report regarding enriched Polymorph C<sub>H</sub> using **VI** noted boron under hydroxide conditions was required for ordering. These reports indicate a variety of inorganic conditions in both fluoride and hydroxide conditions must be screened in attempts to synthesize enriched products.

In addition to the enriched Beta examples above other reports of Beta products enriched in various polymorphs have appeared. A series of materials denoted NCL-5, NCL-6 and NCL-7 claim polymorph B enrichment<sup>33, 34</sup>. These materials were synthesized using tetraethylammonium fluoride with perchloric acid added as a nucleation promoter, although a recent publication argued that the experimental evidence was consistent with BEC enrichment instead<sup>32</sup>. Another report used tetraethylammonium hydroxide and chiral Rhodium complexes or alkaloids under acidic fluoride conditions (pH~4) to “recrystallize” Beta. The authors deconvoluted the broad low angle reflection shown in Figure 3.2 to calculate relative polymorph A/B ratios and claimed partial polymorph A enrichment<sup>35</sup>. The authors noted that no products gave a reflection at  $\sim 9.7^\circ 2\theta$  that would provide clear evidence of polymorph A.



### 3.2: Experimental Section

#### 3.2.1: Structure Directing Agent Synthesis

All reagents were purchased from commercial vendors and were used as received. SDAs were synthesized according to published procedures<sup>17, 19</sup> and purified using the methodologies outlined in Chapter Two. Specific optical rotation measurements were performed using a Jasco P-2000 Polarimeter. Liquid NMR spectra were recorded on 300 MHz Varian Mercury spectrometers. Combustion analysis was performed at the Chevron Energy Technology Center (Richmond, CA) using a Carlo-Erba Combustion Elemental Analyzer. All SDAs were exchanged to the hydroxide form using Dowex Monosphere 550A UPW hydroxide resin (Supelco). Final hydroxide concentration was determined by titration with 0.01N HCl solution to a phenolphthalein end point.

1,3-bis((S)-3,3-dimethylbutan-2-yl)imidazolium chloride (**17**): Using (S)-3,3-dimethyl-2-butylamine (2x121 mmol; Alfa-Aesar, 99+%, ee 99+%) and activated carbon purification, 8.81 g white solids (32.3 mmol, 27% yield) were obtained. <sup>1</sup>H NMR (300 MHz, DMSO-d<sub>6</sub>): 9.77, 7.94, 4.39, 1.49, 0.87. <sup>13</sup>C NMR (75 MHz, DMSO-d<sub>6</sub>): 136.0, 121.7, 64.3, 34.5, 25.9, 14.7. Analysis calculated for C<sub>15</sub>H<sub>29</sub>ClN<sub>2</sub>: C, 66.03; H, 10.71; N, 10.27 (C/N=6.43). Observed C, 64.24; H, 10.72; N, 10.07 (C/N=6.38).  $[\alpha]_D^{25} = -5.33$  (c=14.4, H<sub>2</sub>O) (after ion-exchange to the hydroxide form).

1,3-bis((S)-1-phenylethyl)imidazolium tetrafluoroborate (**18**): Using (S)-(-)-1-phenylethylamine (2x73 mmol; Alfa-Aesar, 99+%, ee 99.5%) followed by recrystallization from ethyl acetate/dichloromethane to give 13.93g off-white solids (38.3

mmol, 52% yield).  $^1\text{H}$  NMR (300 MHz, DMSO- $d_6$ ): 9.71, 7.96, 7.44–7.37, 5.81, 1.90.  $^{13}\text{C}$  NMR (75 MHz, DMSO- $d_6$ ): 139.6, 134.8, 129.1, 128.7, 126.6, 121.6, 58.9, 20.4. Analysis calculated for  $\text{C}_{19}\text{H}_{21}\text{BF}_4\text{N}_2$ : C, 62.66; H, 5.81; N, 7.69 (C/N=8.15). Observed C, 64.68; H, 6.21; N, 7.99 (C/N=8.10).  $[\alpha]_D^{25} = -17.5$  ( $c=1.18$ ,  $\text{CHCl}_3$ ).  $[\alpha]_D^{20} = +18.5$  ( $c=0.96$ ,  $\text{CHCl}_3$ ) reported for 1,3-bis-((R)-1-phenylethyl)imidazolium tetrafluoroborate<sup>19</sup>.

1,3-bis((S)-1-cyclohexylethyl)imidazolium tetrafluoroborate (**19**): Using (S)-(+)-1-cyclohexylethylamine (2x98 mmol, Alfa-Aesar, 98%, ee 97+%) followed by recrystallization from ethyl acetate to give 14.65g pale tan crystals (38.9 mmol, 40% yield).  $^1\text{H}$  NMR (300 MHz, DMSO- $d_6$ ): 9.27, 7.90, 4.26, 1.74–1.63, 1.49, 1.22–1.04, 0.97–0.81.  $^{13}\text{C}$  NMR (75 MHz, DMSO- $d_6$ ): 134.5, 121.2, 60.9, 42.4, 28.6, 28.4, 25.6, 25.3, 25.1, 17.4. Analysis calculated for  $\text{C}_{19}\text{H}_{33}\text{BF}_4\text{N}_2$ : C, 60.65; H, 8.84; N, 7.44 (C/N=8.15). Observed C, 61.09; H, 8.64; N, 7.45 (C/N=8.20).  $[\alpha]_D^{25} = -7.90$  ( $c=1.01$ ,  $\text{CHCl}_3$ ).  $[\alpha]_D^{22} = +11.2$  ( $c=1.0$ ,  $\text{CHCl}_3$ ) reported for 1,3-bis((R)-1-cyclohexylethyl)imidazolium chloride<sup>21</sup>.

1,3-bis((S)-1-cyclohexylpropyl)imidazolium bromide (**20**): (S)-1-cyclohexylpropylamine was obtained via hydrogenation of (S)-(-)-1-phenylpropylamine (187.2 mmol, Alfa-Aesar, 99+%, ee 99%) using a Parr shaker apparatus<sup>36, 37</sup>. Partial hydrogenation was observed using 5% Rh/ $\text{Al}_2\text{O}_3$  under acidic aqueous conditions (pH~1) at 50 psi  $\text{H}_2$  over approximately 40 hours at room temperature<sup>3</sup>. The catalyst was filtered off and the aqueous solution made basic with sodium hydroxide. The basic solution was extracted with diethyl ether, dried over  $\text{Na}_2\text{SO}_4$  filtered and concentrated by rotary evaporation. The crude phenyl + cyclohexyl mixture was further hydrogenated using

<sup>3</sup> No reaction was observed under 1 atmosphere  $\text{H}_2$  in contrast to the report in Reference 4.

PtO<sub>2</sub> in acetic acid at 50 psi H<sub>2</sub> in approximately 12 hours. After careful catalyst separation via filtration, 6N sodium hydroxide solution was added to pH>12. The aqueous phase was extracted with diethyl ether (3x100 mL). The combined organic extracts were washed with brine, dried over Na<sub>2</sub>SO<sub>4</sub>, filtered and concentrated by rotary evaporation to give 25.2 g clear, colorless (S)-1-cyclohexylpropylamine (178.6 mmol, 95% yield). <sup>1</sup>H NMR (300 MHz, CDCl<sub>3</sub>): 2.29, 1.67–1.65, 1.62–1.52, 1.39, 1.18–1.09, 1.07–0.90, 0.81. <sup>13</sup>C NMR (75 MHz, CDCl<sub>3</sub>): 57.5, 43.3, 29.7, 27.8, 27.3, 26.6, 26.5, 26.4, 10.8.

Imidazolium synthesis was performed using (S)-1-cyclohexylpropylamine from above (2x85.0 mmol). The crude product was recrystallized in several crops from 1:1 methanol/ethyl acetate at -18°C using just enough diethyl ether to give a cloudy solution. The combined crops gave 19.35 g white to off-white crystals (48.7 mmol, 57% yield). <sup>1</sup>H NMR (300 MHz, CDCl<sub>3</sub>): 10.80, 7.38, 4.32, 3.43, 2.07–2.01, 1.94–1.63, 1.25–0.92, 0.78. <sup>13</sup>C NMR (75 MHz, CDCl<sub>3</sub>): 138.0, 120.3, 68.4, 42.2, 30.0, 29.0, 25.9, 25.8, 25.7, 25.0, 10.5. Analysis calculated for C<sub>21</sub>H<sub>37</sub>BrN<sub>2</sub>: C, 63.46; H, 9.38; N, 7.05 (C/N=9.00). Observed C, 62.94; H, 9.57; N, 7.07 (C/N=8.90). [ $\alpha$ ]<sub>D</sub><sup>25</sup> = -22.42 (c=1.21, CHCl<sub>3</sub>).

1,3-bis(((1S,2S,5R)-6,6-dimethylbicyclo[3.1.1]heptan-2-yl)methyl)imidazolium tetrafluoroborate (**21**) (1,3-bis(cis-Myrtanyl)imidazolium tetrafluoroborate): The procedure for bis(cyclopentyl) SDA **7** in Chapter Two was adapted using (-)-cis-Myrtanylamine (2x32.6 mmol, Sigma-Aldrich, 98%). The crude reaction layers were separated after adding 50 mL diethyl ether and 10 mL saturated KHCO<sub>3</sub> solution plus 20 mL water. The aqueous layer plus oily residue were extracted with chloroform (3x35 mL). Organic extracts were combined and washed with brine (50 mL), dried over

MgSO<sub>4</sub>, filtered and stripped down by rotary evaporation to obtain a dark, viscous oil. Further drying under high vacuum yielded a waxy residue. Ethyl acetate (30 mL) was added to the residue and sonication (2x15 minutes) separated a small quantity of pale solids. Diethyl ether (~50 mL) was slowly added until the supernatant became cloudy then the flask was moved to a 4°C refrigerator. Filtration and subsequent drying under high-vacuum gave 9.51 g pale tan solids (22.2 mmol, 68% yield). <sup>1</sup>H NMR (300 MHz, DMSO-d<sub>6</sub>): 9.58, 8.01, 4.29, 3.50, 2.72–2.66, 2.05–1.95, 1.87, 1.72 – 1.69, 1.34, 1.25, 1.06. <sup>13</sup>C NMR (75 MHz, CDCl<sub>3</sub>): 136.3, 122.6, 54.0, 42.6, 41.0, 40.5, 38.2, 32.3, 27.5, 25.2, 22.9, 18.2. Analysis calculated for C<sub>23</sub>H<sub>37</sub>BF<sub>4</sub>N<sub>2</sub>: C, 64.49; H, 8.71; N, 6.54 (C/N=9.86). Observed C, 66.09; H, 8.62; N, 6.66 (C/N=9.93). [ $\alpha$ ]<sub>D</sub><sup>25</sup> = -13.44(c=1.15, CHCl<sub>3</sub>).

### 3.2.2: Inorganic Reactions

All reactions were performed in 23mL PTFE-lined stainless steel autoclaves (Parr Instruments). Hydroxide mediated reactions were tumbled at approximately 40 rpm using spits built into convection ovens. Fluoride mediated reactions were not tumbled. Silica sources were tetraethylorthosilicate (TEOS, Sigma-Aldrich, 98%) for fluoride reactions and Cab-O-Sil M5 fumed silica (Cabot) for hydroxide reactions. Boric acid (J.T. Baker, ACS Reagent) was used for borosilicate reactions and Reheis F-2000 aluminum hydroxide gel (50–53 wt% Al<sub>2</sub>O<sub>3</sub>) or NaY zeolite (Tosoh HSZ-320NAA) was used in aluminosilicate reactions. All reactions were performed at 150°C unless otherwise noted. B-Beta was provided by S.I. Zones (Chevron Energy Technology Company, Richmond, CA) and

calcined under nitrogen with a small amount of air to minimize boron hydrolysis. Germanosilicate reactions used TEOS and germanium dioxide (Alfa-Aesar, 99.98%). Silicoaluminophosphate (SAPO) reactions used Cab-O-Sil M5, Reheis F-2000 and 85wt% phosphoric acid (Fisher, ACS Reagent) as silicon, aluminum and phosphorus sources respectively. SAPO gels were prepared by combining silica with  $\text{SDA}^+\text{OH}^-$  solution then adding to the aluminophosphate gel. The combined gel was homogenized then aged overnight at room temperature.

### 3.2.3: Molecular Modeling

Cerius<sup>2</sup> (Molecular Simulations Inc./Accelrys Software Inc.) was used for molecular modeling. Inorganic frameworks built into the software were used without modification. Framework atom positions and unit cell dimensions were fixed during energy minimizations. All energy minimizations employed the Burchart-Universal Force-Field<sup>38, 39</sup>. Coulombic interactions between the silicate framework and SDA were not included<sup>40</sup>. Reported stabilization energies represent the computed energy difference between the free SDA and the SDA occluded within the silicate framework, normalized by the number of tetrahedral atoms. In general, several SDA starting locations were tried for each guest/host pair although no attempt was made to exhaustively search for global energy minima.

### 3.2.4: Product Characterization

Powder X-ray diffraction (XRD) patterns were collected on a Scintag XDS-2000 diffractometer equipped with scintillation detector using  $\text{CuK}\alpha$  radiation. Thermogravimetric analysis (TGA) was performed using a Netzsch STA449C instrument under  $75 \text{ mL min}^{-1}$  air plus  $25 \text{ mL min}^{-1}$  Argon at a heating rate of  $5^\circ\text{C min}^{-1}$ . Solid-state NMR spectra were collected using either Bruker Avance 200MHz or Bruker DSX 500 MHz instruments. Scanning electron microscopy (SEM) was performed using a JEOL JSM-6700F instrument. Elemental analyses were performed by Galbraith Laboratories (Knoxville, TN).

### 3.3: Results and Discussion

To investigate the synthesis of zeolite Beta enriched in polymorph A an initial reaction screen was performed using all five chiral SDAs. Three water to silica ratios in pure silica fluoride reactions were performed for all SDAs and at least one boron or aluminum rich hydroxide reaction was attempted. Similar reaction conditions studied in Chapter Two yielded many instances of Beta. Not all hydroxide conditions were studied for each SDA due to reduced SDA quantity. The phases obtained in pure silica fluoride reactions are reported in Table 3.2 while borosilicate and aluminosilicate reaction results are presented in Table 3.3.

Results from pure silica fluoride reactions in Table 3.2 only show five instances of crystalline products. The crystalline products were obtained with two SDAs (**17** and **19**).

Pleasingly, three of these five contained Beta as the major product. Discovering two chiral SDAs capable of synthesizing Beta was promising as published studies using chiral SDAs only showed one instance of Beta as discussed in Section 3.1. The two remaining instances showed Beta and EU-1 (EUO) using **17**. The XRD pattern of the Beta product obtained using **17** at  $\text{H}_2\text{O}/\text{SiO}_2=3.5$  showed distinct differences in the low angle reflection compared with a typical Beta pattern. The distinct asymmetry in the low angle reflection did not correspond to any simulated XRD patterns for polymorph A/polymorph B intergrowths. Figure 3.4 shows the XRD patterns for Beta products obtained using **17** and **19** at  $\text{H}_2\text{O}/\text{SiO}_2=3.5$ .

The phases obtained from hydroxide reactions presented in Table 3.3 again show crystalline products were limited to **17** and **19**. Beta was the major product in four of the five reactions that gave crystalline products. Two unusual Beta XRD patterns were observed using **19** with boron and aluminum lattice substitution. In contrast to the pure silica fluoride reactions the one Beta instance using **17** gave a regular Beta pattern. EU-1 was observed as the major product under borosilicate conditions using **17** and as an impurity under aluminosilicate conditions. Figure 3.5 shows XRD patterns for borosilicate products obtained using **17** and **19**.

Table 3.2: Phases obtained in pure silica fluoride reactions using chiral imidazolium

SDAs			
SDA	$H_2O/SiO_2$		
	3.5	7.5	14.5
<b>17</b>	Beta (odd) <sup>a</sup>	Beta + EU-1 <sup>a</sup>	EU-1 (Beta) <sup>a</sup>
<b>18</b>	Amorphous	Amorphous	Amorphous
<b>19</b>	Beta	Beta	Amorphous
<b>20</b>	Amorphous <sup>a</sup>	Amorphous <sup>a</sup>	Amorphous <sup>a</sup>
<b>21</b>	Amorphous	Amorphous	Amorphous

<sup>a</sup> Reaction performed at 175°C

The odd Beta XRD patterns obtained using **17** and **19** were investigated further and close inspection of the XRD patterns presented in Reference 41 (top pattern in Figure 3 and lower patterns in Figure 4) shows clear similarities to the patterns obtained above and those reported for SDA labeled “MBABO<sup>+</sup>” (6-benzyl-1,3,3,6-tetramethyl-6-azoniabicyclo[3.2.1]octane) and several described as Beta/SSZ-31 intergrowths. The authors grouped the distinct Beta product with typical Beta products as additional <sup>19</sup>F NMR analysis showed no evidence of resonances typical of fluoride residing in D4R cages. The product obtained from the concentrated fluoride reaction with **17** was analyzed by <sup>19</sup>F MAS NMR and a small resonance at -37.0 ppm was visible in addition to the dominant resonance at -70.6 ppm (relative intensity 1.0:18.1). The -37 ppm resonance is characteristic of fluoride residing in D4Rs and therefore this material probably contains some BEC. This could partially explain the observed diffraction pattern, although the quantity of D4Rs indicated by <sup>19</sup>F MAS NMR was lower than those reported to show changes in XRD



patterns. For the odd Beta patterns from hydroxide reactions  $^{19}\text{F}$  NMR was not possible and therefore a clear signature was not available to conclusively assign the intergrowth.

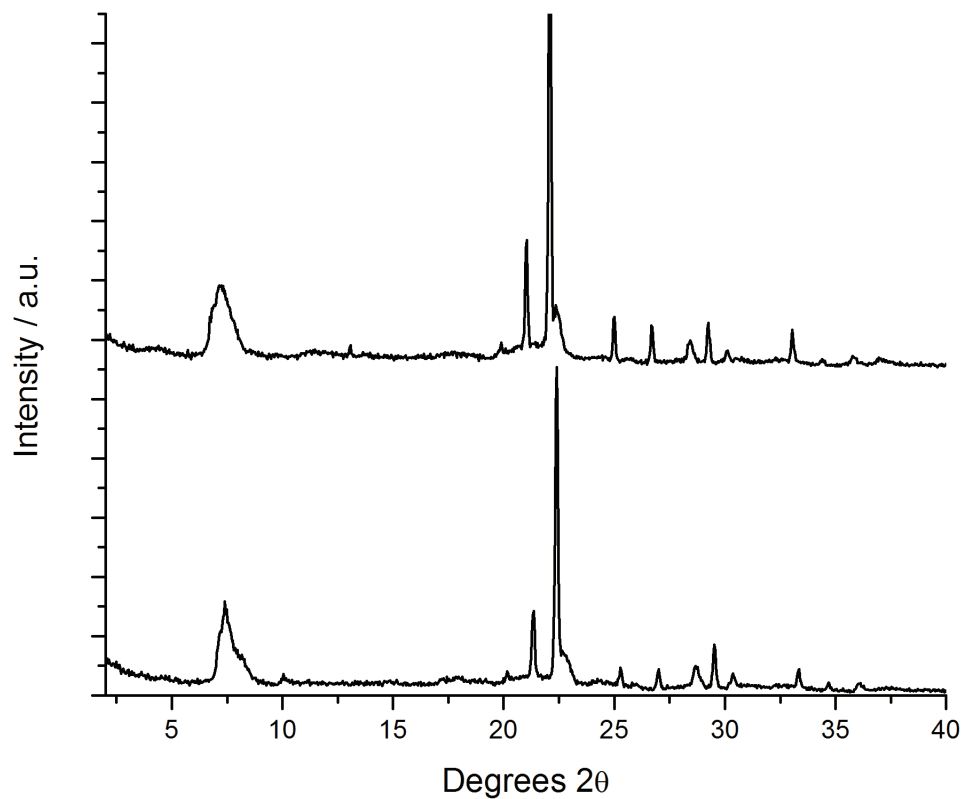


Figure 3.4: XRD patterns of pure silica Beta products using **17** and **19** at  $\text{H}_2\text{O}/\text{SiO}_2=3.5$ .

Top=regular Beta obtained with **19** and bottom=odd Beta pattern using **17** with distinct asymmetry in the low angle reflection

Table 3.3: Phases obtained in aluminosilicate and borosilicate hydroxide reactions using  
chiral imidazolium SDAs

SDA	$\text{SiO}_2/\text{Al}_2\text{O}_3=35$ (NaY reaction)	$\text{SiO}_2/\text{Al}_2\text{O}_3=50$	$\text{SiO}_2/\text{B}_2\text{O}_3 \leq 30$
<b>17</b>	NR	Beta (EU-1)	EU-1 (layered)
<b>18</b>	Amorphous	Amorphous	Amorphous
<b>19</b>	Beta	Beta (odd)	Beta (odd)
<b>20</b>	NR	Amorphous	Amorphous
<b>21</b>	Amorphous (FAU)	NR	NR

NR indicates reaction not run

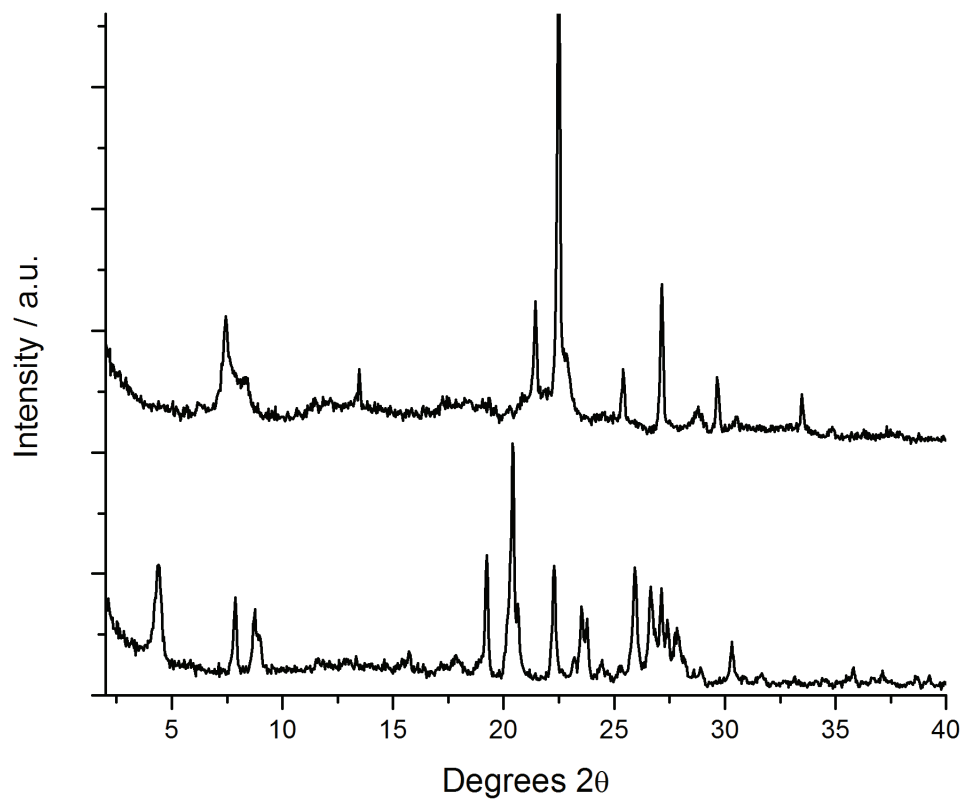


Figure 3.5: Borosilicate hydroxide XRD patterns. Top=Beta with asymmetry in the low  
angle reflection using **19** and bottom shows EU-1 plus minor layered using **17**

The initial inorganic reaction matrix gave very promising results with **17** and **19** while the remaining three SDAs gave no crystalline products. This was particularly perplexing in the case of **18** as the SDA was almost identical to **19** that exhibited strong specificity to Beta materials. The inability of **20** and **21** to form products could be due to higher hydrophobicity. Although bis(adamantyl) SDA **15** studied in Chapter Two produced three crystalline phases, it could be argued that this arose from the unique properties of the adamantyl groups (bulky, rigid and hydrothermally stable). Therefore, while it was possible to synthesize crystalline products using **15** with  $\Sigma(C+N)=25$  this may represent an exceptional case. In light of this, no additional reactions were attempted with **20** and **21** while independent studies were undertaken using **18** and **19**. The additional reactions using **18** were aimed at producing any crystalline phase, whereas those with **19** were aimed at perturbing the reaction environment such that polymorph A enriched Beta might be obtained.

Table 3.4 summarizes additional reactions performed with **19** in attempts to obtain polymorph A enriched Beta. The first group was additional fluoride reactions (Entries 1–5). Entries 1–4 added aluminum or boron to the gel to probe the role framework charge might have on the product phase. The aluminosilicate and borosilicate hydroxide reactions with this SDA gave several instances of the odd Beta pattern in contrast to pure silica reactions that did not. Therefore, it was hypothesized that framework charge introduced by aluminum or boron substitution might be responsible for the observed XRD patterns. These reactions gave amorphous products for all aluminosilicate reactions while regular Beta was obtained with boron addition. Entries 1–3 were particularly intriguing as aluminum addition completely suppressed product formation at all water to silica ratios.

The  $\text{H}_2\text{O}/\text{SiO}_2=3.5$  reaction was particularly surprising as low water content and aluminum introduction separately favor formation of open structures with low framework density, with Beta being particularly common. Entry 5 used the inorganic conditions Cantín et al. employed to synthesize pure silica BEC using Diels-Alder SDA **VII**<sup>12</sup>. Under these conditions only  $\text{K}_2\text{SiF}_6$  was observed.

Entries 6-13 were aluminosilicate or borosilicate hydroxide reactions with perturbations to the gel composition. The first group (6–10) employed seeding in attempts to induce polymorph A nucleation and growth. Seeding often increases product formation rate as suitable nuclei for crystal growth are introduced into the reaction gel. In addition, seeding can improve product purity by suppressing growth of competing phases. In this regard, polymorph B and one polymorph A intergrowth could be viewed as competing phases to the desired enantiopure polymorph A structure. All five entries gave Beta, and all four borosilicate reactions gave the odd Beta pattern presented in Figures 3.4 and 3.5. Interestingly, no asymmetry was observed in the seeded aluminosilicate reaction (Entry 10). Seeded reactions at 150°C gave faster product formation, e.g., Entry 6 showed nice phase separation after four days whereas the unseeded reaction required 18 days. Entries 6–8 also explored seeded reactions at different temperatures to investigate if lower thermal energy could lead to polymorph A enrichment. The results showed the same XRD pattern at each temperature. Similarly, substituting KOH for NaOH did not alter the product XRD pattern.

The final subset added chiral amino alcohols to perturb the reaction gel. Gel compositions were modeled after those employed to synthesize SSZ-25 using a mixed quaternary ammonium/amine system<sup>42</sup>. Leucine- and proline-derived amino alcohols (S)-

leucinol and (S)-1-methyl-2-pyrrolidinemethanol were used as chiral additives. No effect was observed in the aluminosilicate reaction whereas quartz and quartz plus minor Beta were obtained under borosilicate conditions. This approach did not have any positive effect so was not investigated further.

The final reactions undertaken were aimed at synthesizing a one dimensional product that could have a helical pore. The two reactions were at  $\text{SiO}_2/\text{Al}_2\text{O}_3=100$  and  $\infty$  respectively. The SAR=100 gave Beta while the pure silica reaction gave quartz. These results are in agreement with those observed using bis(cyclooctyl) SDA **13** in Chapter Two where Beta was observed under all conditions except pure silica hydroxide. With no trivalent lattice substitution both SDAs were unable to crystallize Beta.

Table 3.4: Summary of additional inorganic reaction attempts using **19**

Entry	Gel Composition	Phase
<b>1</b>	1.0SiO <sub>2</sub> :0.02Al <sub>2</sub> O <sub>3</sub> :0.5SDA <sup>+</sup> OH <sup>-</sup> :0.5HF:3.0H <sub>2</sub> O	Amorphous
<b>2</b>	1.0SiO <sub>2</sub> :0.02Al <sub>2</sub> O <sub>3</sub> :0.5SDA <sup>+</sup> OH <sup>-</sup> :0.5HF:7.0H <sub>2</sub> O	Amorphous
<b>3</b>	1.0SiO <sub>2</sub> :0.02Al <sub>2</sub> O <sub>3</sub> :0.5SDA <sup>+</sup> OH <sup>-</sup> :0.5HF:14.0H <sub>2</sub> O	Amorphous
<b>4</b>	1.0SiO <sub>2</sub> :0.05B <sub>2</sub> O <sub>3</sub> :0.5SDA <sup>+</sup> OH <sup>-</sup> :0.5HF:7.0H <sub>2</sub> O	Beta
<b>5</b>	1.0SiO <sub>2</sub> :0.5SDA <sup>+</sup> OH <sup>-</sup> :0.25KOH:0.5HF:7.25H <sub>2</sub> O	K <sub>2</sub> SiF <sub>6</sub>
<b>6</b>	1.0SiO <sub>2</sub> :0.03B <sub>2</sub> O <sub>3</sub> :0.2SDA <sup>+</sup> OH <sup>-</sup> :0.1NaOH:50.0H <sub>2</sub> O <sup>a</sup>	Beta (odd)
<b>7</b>	1.0SiO <sub>2</sub> :0.03B <sub>2</sub> O <sub>3</sub> :0.2SDA <sup>+</sup> OH <sup>-</sup> :0.1NaOH:50.0H <sub>2</sub> O <sup>a,b</sup>	Beta (odd)
<b>8</b>	1.0SiO <sub>2</sub> :0.03B <sub>2</sub> O <sub>3</sub> :0.2SDA <sup>+</sup> OH <sup>-</sup> :0.1NaOH:50.0H <sub>2</sub> O <sup>a,c</sup>	Beta (odd)
<b>9</b>	1.0SiO <sub>2</sub> :0.03B <sub>2</sub> O <sub>3</sub> :0.2SDA <sup>+</sup> OH <sup>-</sup> :0.1KOH:50.0H <sub>2</sub> O <sup>a</sup>	Beta (odd)
<b>10</b>	1.0SiO <sub>2</sub> :0.02Al <sub>2</sub> O <sub>3</sub> :0.2SDA <sup>+</sup> OH <sup>-</sup> :0.1KOH:40.0H <sub>2</sub> O <sup>d</sup>	Beta
<b>11</b>	1.0SiO <sub>2</sub> :0.03B <sub>2</sub> O <sub>3</sub> :0.1SDA <sup>+</sup> OH <sup>-</sup> :0.1NaOH:0.2amine <sup>e</sup> :50.0H <sub>2</sub> O <sup>a</sup>	Quartz
<b>12</b>	1.0SiO <sub>2</sub> :0.03B <sub>2</sub> O <sub>3</sub> :0.1SDA <sup>+</sup> OH <sup>-</sup> :0.1NaOH:0.2amine <sup>f</sup> :50.0H <sub>2</sub> O <sup>a</sup>	Quartz (Beta)
<b>13</b>	1.0SiO <sub>2</sub> :0.02Al <sub>2</sub> O <sub>3</sub> :0.1SDA <sup>+</sup> OH <sup>-</sup> :0.1NaOH:0.2amine <sup>e</sup> :50.0H <sub>2</sub> O <sup>d</sup>	Beta
<b>14</b>	1.0SiO <sub>2</sub> :0.01Al <sub>2</sub> O <sub>3</sub> :0.15SDA <sup>+</sup> OH <sup>-</sup> :0.1KOH:40.0H <sub>2</sub> O <sup>g</sup>	Beta
<b>15</b>	1.0SiO <sub>2</sub> :0.00Al <sub>2</sub> O <sub>3</sub> :0.15SDA <sup>+</sup> OH <sup>-</sup> :0.1KOH:40.0H <sub>2</sub> O <sup>g</sup>	Quartz

<sup>a</sup>Added calcined B-Beta seeds<sup>b</sup>Reaction performed at 135°C<sup>c</sup>Reaction performed at 115°C<sup>d</sup>Added calcined Beta seeds<sup>e</sup>Added (S)-1-methyl-2-pyrrolidinemethanol as chiral amine<sup>f</sup>Added (S)-leucinol as chiral amine<sup>g</sup>Performed at 160°C

The combined results presented in Tables 3.2–3.4 show many instances of Beta using SDAs **17** and **19** and several show asymmetry in the low angle XRD reflection. Further analysis was performed on the solid products in attempts to gain insight into the differences in XRD patterns. Thermogravimetric analysis (TGA) was performed on solids

obtained from reactions discussed above. Nine products were selected encompassing amorphous, Beta and Beta with asymmetric low angle reflections (“odd” Beta). Table 3.5 presents the mass loss between 200 and 620°C. This temperature range broadly measures the organic content occluded within the silicate host. Any mass loss below 200°C was assigned to bound water with many pure silica fluoride products showing negligible mass loss < 200°C (<0.5 wt%).

The organic content for both aluminosilicate fluoride reactions using **19** at  $\text{H}_2\text{O}/\text{SiO}_2=3.5$  and 7.5 was low at 6.6 and 6.5 wt% respectively. The reported mass loss also includes any fluorine bonded to silica. The low organic content suggests aluminum addition created unfavorable organic/silicate interactions thereby preventing nucleation. In comparison, the eight reactions yielding Beta show mass loss ranging from 22.1 to 17.5 wt%. The measured mass loss for the four fluoride reactions includes fluorine bonded to silica. This complicates the analysis as 1–2 wt% fluorine was expected based on elemental analyses presented in Chapter Two. The remaining Beta products contain no fluorine and show subtle differences in organic content. Products with odd Beta XRD patterns show slightly higher organic content compared to the normal Beta product. This suggests the odd XRD pattern may result from slightly higher organic content in certain Beta products.

Table 3.5: Thermogravimetric analysis of inorganic reaction products using **17** and **19**

Phase	SDA	Notes	Mass loss / wt%
Amorphous	<b>19</b>	Aluminosilicate fluoride, H <sub>2</sub> O/SiO <sub>2</sub> =3.5	6.6
Amorphous	<b>19</b>	Aluminosilicate fluoride, H <sub>2</sub> O/SiO <sub>2</sub> =7.5	6.5
Beta (odd)	<b>17</b>	Pure silica fluoride, H <sub>2</sub> O/SiO <sub>2</sub> =3.5	22.1
Beta	<b>17</b>	Aluminosilicate hydroxide, NaOH	18.4
Beta	<b>19</b>	Pure silica fluoride, H <sub>2</sub> O/SiO <sub>2</sub> =3.5	21.1
Beta	<b>19</b>	Pure silica fluoride, H <sub>2</sub> O/SiO <sub>2</sub> =7.5	20.6
Beta	<b>19</b>	Borosilicate fluoride, H <sub>2</sub> O/SiO <sub>2</sub> =7.5	19.0
Beta (odd)	<b>19</b>	Borosilicate hydroxide, seeded, NaOH	18.4
Beta (odd)	<b>19</b>	Borosilicate hydroxide, seeded, KOH	19.3
Beta	<b>19</b>	Aluminosilicate hydroxide, seeded, KOH	17.5

In addition, solid-state NMR analysis was performed to ensure the occluded organic was intact. Figures 3.6 and 3.7 show <sup>13</sup>C cross-polarization magic-angle spinning (CP-MAS) NMR of Beta products obtained using **19** and **17** respectively. Both figures include the <sup>13</sup>C liquid NMR spectra of the parent salt recorded in deuterated dimethyl sulfoxide. Both figures show evidence of imidazolium carbon resonances at ~135 and 120 ppm and alkyl carbons between 65 and 10 ppm. The imidazolium resonances are broad due to less efficient cross-polarization and/or constrained motion. These spectra are in agreement with the parent SDA spectra. The top spectrum in Figure 3.6 shows two resonances at 125 and 121 ppm whereas the other spectra do not show this. The ~120 ppm resonance in liquid <sup>13</sup>C spectra arises from the C(4) and C(5) carbons of the imidazolium ring. Observing apparent splitting suggests these carbons may reside in different environments within the host framework. A similar observation was noted for 1,4-diazabicyclo[2.2.2]octane-



derived quaternary polymer molecules residing in gmelinite (GME)<sup>43</sup>. In contrast to the apparent splitting observed for **19**, one resonance at ~121 ppm was observed for **17**. The spectrum for **17** occluded within Beta shows relatively sharp imidazolium resonances compared to those for **19**. This could be due to greater mobility within the channels for the smaller SDA **17**.

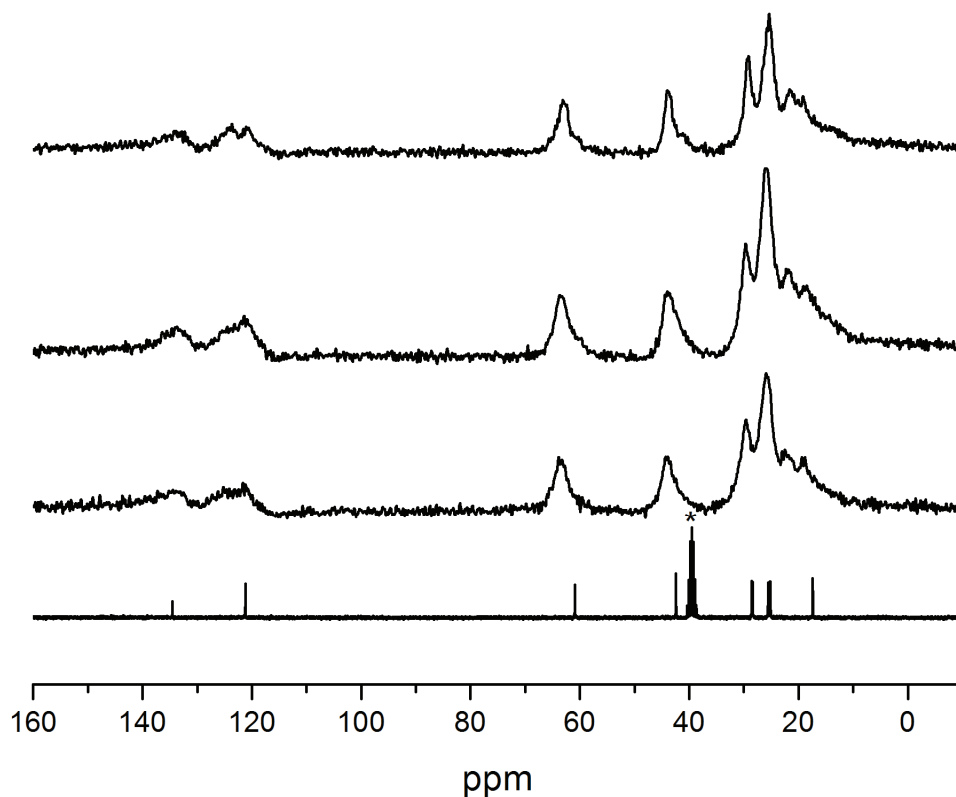


Figure 3.6:  $^{13}\text{C}$  CP-MAS NMR of Beta products using **19**. Top to bottom: Pure silica fluoride at  $\text{H}_2\text{O}/\text{SiO}_2=3.5$ , aluminosilicate hydroxide (SAR=50), borosilicate hydroxide (seeded) and liquid  $^{13}\text{C}$  NMR of tetrafluoroborate salt (asterisk denotes NMR solvent resonances)

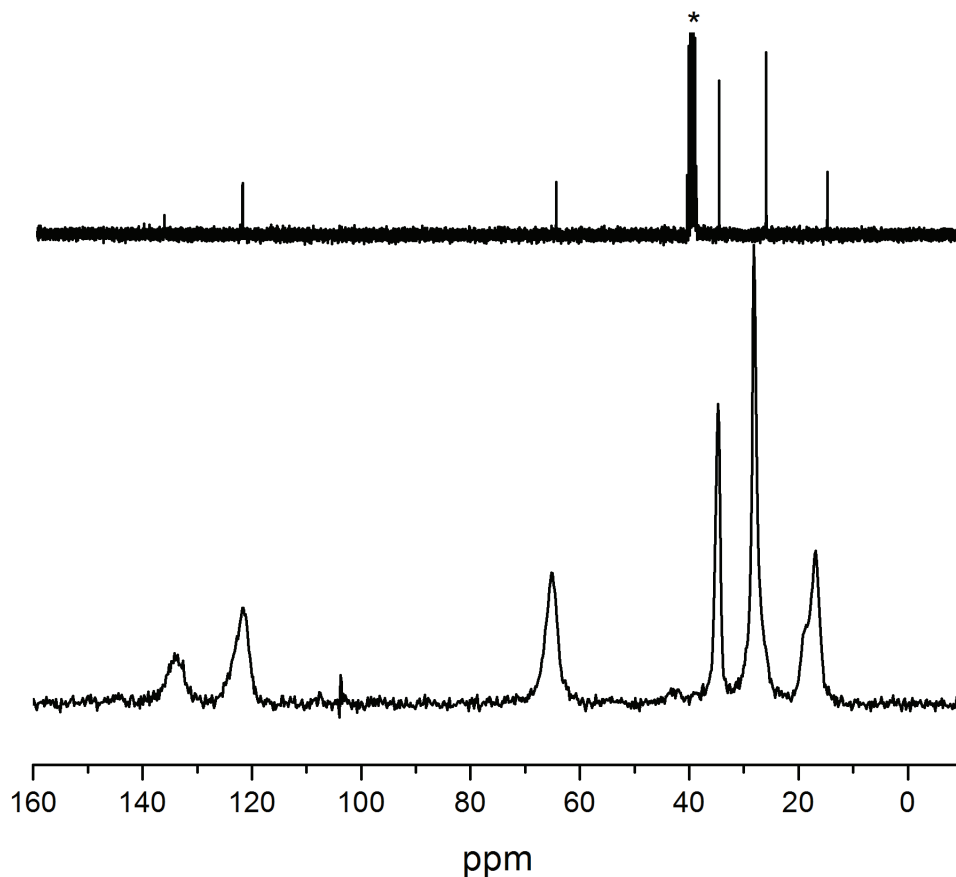


Figure 3.7:  $^{13}\text{C}$  CP-MAS NMR of Beta products using **17**. Top spectra shows liquid  $^{13}\text{C}$  NMR of chloride salt (asterisk denotes NMR solvent resonances) and bottom shows  $^{13}\text{C}$  CP-MAS NMR of Beta product

Table 3.6 presents the additional inorganic reactions attempted using **18**. Entries 1 and 2 used calcined boron-Beta (B-Beta) either as the entire source of tetrahedral atoms (Si and B, 1) or as seed material (2). The gel composition for the B-Beta transformation was based on reported conditions where rapid transformations to a variety of products occurred<sup>44</sup> while the seeded reaction was as reported in Table 3.4. Beta was observed by XRD after 39 days at 150°C for the B-Beta reaction. This implied the SDA occupied the

void volume within the framework thereby preventing dissolution. TGA of the recovered product gave 17.7 wt% mass loss between 200 and 620°C confirming organic occlusion. In contrast, the addition of B-Beta seeds to an unstructured borosilicate gel resulted in layered product formation. This was in stark contrast to the entries in Table 3.4 using **19** where seeded reactions yielded rapid Beta formation.

A collection of reactions with varying aluminum content was considered next (Entries 3–5). Entry 3 repeated the NaY reaction reported in Table 3.2 but with additional NaOH ( $\text{NaOH}/\text{SiO}_2=0.4$  *cf* 0.1 in Table 3.2). Entries 4 and 5 used the same gel compositions as Entries 14 and 15 in Table 3.4 in a similar attempt to synthesize one-dimensional products. The three reactions gave Mordenite (MOR), layered and quartz respectively. As discussed in Chapter Two, MOR appears very frequently in NaY reactions with increasing  $\text{Na}^+$  content and can be considered the default product. Obtaining layered material and quartz from the low aluminum reactions also suggests unfavorable organic/silicate interactions with both phases undesirable.

The final reaction collection explored germanosilicate reactions as germanium incorporation has led to the discovery of many new materials. Germanium inclusion often directs the formation of small cages, with D4Rs very common. Fluoride addition to germanosilicate gels has been shown to accelerate product formation through cooperative stabilization of D4Rs<sup>9</sup>. Three germanosilicate reactions were investigated at  $\text{Si}/\text{Ge}\leq 10$  and low water content ( $\text{H}_2\text{O}/\text{SiO}_2\leq 3.5$ )<sup>45</sup>. The two germanosilicate fluoride reactions (Entries 6 and 7) also included aluminum at  $(\text{SiO}_2+\text{GeO}_2)/\text{Al}_2\text{O}_3=75$  to further enhance the prospect of synthesizing open framework structures. All three reactions yielded amorphous products, with weak  $\text{AlPO}_4$ -16 (AST) reflections visible in the hydroxide reaction. AST is

a clathrate phase constructed entirely of connected D4Rs. The AST cages are not large enough to occlude an intact SDA suggesting minor organic degradation may occur under the synthesis conditions.

Table 3.6: Summary of additional inorganic reaction attempts using **18**

Entry	Gel Composition	Phase
1	1.0SiO <sub>2</sub> :0.03B <sub>2</sub> O <sub>3</sub> :0.15SDA <sup>+</sup> OH <sup>-</sup> :0.1NaOH:30.0H <sub>2</sub> O <sup>a</sup>	Beta
2	1.0SiO <sub>2</sub> :0.03B <sub>2</sub> O <sub>3</sub> :0.2SDA <sup>+</sup> OH <sup>-</sup> :0.1NaOH:50.0H <sub>2</sub> O <sup>b</sup>	Layered
3	1.0SiO <sub>2</sub> :0.029Al <sub>2</sub> O <sub>3</sub> :0.25SDA <sup>+</sup> OH <sup>-</sup> :0.4NaOH:30.0H <sub>2</sub> O <sup>c</sup>	Mordenite
4	1.0SiO <sub>2</sub> :0.01Al <sub>2</sub> O <sub>3</sub> :0.15SDA <sup>+</sup> OH <sup>-</sup> :0.1KOH:40.0H <sub>2</sub> O <sup>d</sup>	Layered
5	1.0SiO <sub>2</sub> :0.00Al <sub>2</sub> O <sub>3</sub> :0.15SDA <sup>+</sup> OH <sup>-</sup> :0.1KOH:40.0H <sub>2</sub> O <sup>d</sup>	Quartz
6	1.0SiO <sub>2</sub> :0.2GeO <sub>2</sub> :0.016Al <sub>2</sub> O <sub>3</sub> :0.6SDA <sup>+</sup> OH <sup>-</sup> :0.6HF:3.6H <sub>2</sub> O	Amorphous
7	1.0SiO <sub>2</sub> :0.1GeO <sub>2</sub> :0.015Al <sub>2</sub> O <sub>3</sub> :0.55SDA <sup>+</sup> OH <sup>-</sup> :0.55HF:3.3H <sub>2</sub> O	Amorphous
8	1.0SiO <sub>2</sub> :0.11GeO <sub>2</sub> :0.50SDA <sup>+</sup> OH <sup>-</sup> :3.5H <sub>2</sub> O <sup>e</sup>	Amorphous(AST)

<sup>a</sup>Calcined B-Beta used as Si and B source

<sup>b</sup>Added calcined B-Beta seeds

<sup>c</sup>NaY reaction at SiO<sub>2</sub>/Al<sub>2</sub>O<sub>3</sub>=35

<sup>d</sup>Performed at 160°C

<sup>e</sup>Performed at 170°C

From the combined inorganic reactions presented above using **18** it was very clear that this SDA was not likely to synthesize a zeolite phase. This shows that very subtle changes to an SDA can effect profound changes on the products obtained. In this case, replacing the cyclohexyl groups of **19** with the phenyl groups of **18** transforms a SDA selective to Beta to one that did not direct the formation of any product. The alkyl-substituted imidazoliums studied by others and presented in Chapter Two were stable under

synthesis conditions while the bis(aryl) SDAs **14** and **16** studied in Chapter Two appeared to degrade significantly faster. For these aryl-substituted imidazoliums, hydroxide attack at the more acidic C(2) proton<sup>46</sup> may have lead to faster degradation. However, reported acidities of benzyl-substituted imidazolium and benzimidazolium salts do not show significantly lower pKa values compared to alkyl substituted salts<sup>46, 47</sup>. To check that the SDA remained intact under synthesis conditions elemental analysis and <sup>13</sup>C CP-MAS NMR were performed.

The amorphous products from pure-silica fluoride reactions using **18** were subjected to elemental analysis for carbon, nitrogen and fluorine. Table 3.7 shows very low organic incorporation for the reactions at higher water to silica ratios. The entry for the concentrated reaction does show ~14 wt% combined carbon, nitrogen and fluorine. In addition, the measured carbon to nitrogen ratio of 7.7 was close to the expected ratio of 8.2. The calculated carbon to nitrogen ratio for the intermediate dilution product was substantially lower than expected for the parent SDA (3.2 *cf* 8.2). This indicates organic degradation occurred for the intermediate dilution reaction, whereas the organic remained substantially intact in the concentrated reaction. These data suggest the SDA was stabilized by the surrounding silicate species under concentrated conditions whereas at higher water dilution the SDA/silicate interaction was not favorable and therefore the SDA was exposed to degradation. In addition, the fluorine/nitrogen weight ratio for the concentrated reaction was 1.51. This was more than double the value expected for SDA<sup>+</sup>F<sup>-</sup> (wt% F/wt% N=0.68) suggesting fluorine-rich silicon species may be present (e.g., [SiF<sub>6</sub>]<sup>2-</sup>). The unusually high fluorine content could explain why no tetrahedral SiO<sub>2</sub> framework was obtained in any reaction.

Table 3.7: Carbon, Nitrogen and Fluorine content of amorphous products from pure silica fluoride reactions **18**

<b>H<sub>2</sub>O/SiO<sub>2</sub></b>	<b>Carbon / wt%</b>	<b>Nitrogen / wt%</b>	<b>Fluorine / wt%</b>	<b>C/N</b>
<b>3.5</b>	10.81	1.40	2.11	7.7
<b>7.5</b>	3.30	1.02	1.52	3.2
<b>14.5</b>	1.44	<0.50	0.91	N/A

In addition to chemical analysis, <sup>13</sup>C CP-MAS NMR was performed on two products using **18**. These were the concentrated pure silica fluoride reaction that showed organic incorporation by elemental analysis and the B-Beta reaction product. Figure 3.8 shows the liquid <sup>13</sup>C NMR of the parent tetrafluoroborate salt in addition to the <sup>13</sup>C CP-MAS NMR spectra for each product. Aromatic and alkyl resonances are visible for each product and agree with those of the parent SDA. This confirms the SDA did not degrade significantly under these two reaction conditions.

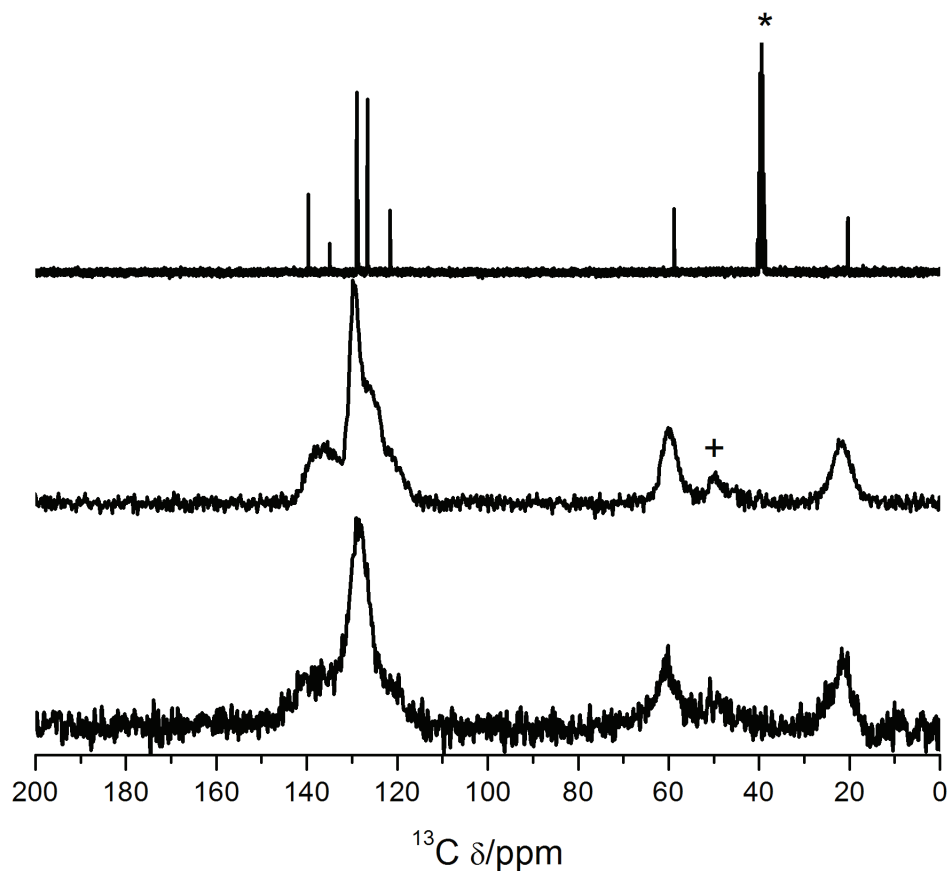


Figure 3.8: Liquid  $^{13}\text{C}$  NMR of SDA **18** and  $^{13}\text{C}$  CP-MAS NMR of products using **18**.

Top to bottom=liquid NMR spectrum, B-Beta reaction product and pure-silica product at  $\text{H}_2\text{O}/\text{SiO}_2=3.5$ . \* denotes resonances from the NMR solvent and + indicates spinning side-band.

The additional investigations with **19** did not reveal instances of polymorph A enriched Beta. Without any success in crystallizing an enriched chiral product in high silica chemistry, silicoaluminophosphate (SAPO) reactions were explored using **17** and **19**. In contrast to the inorganic reactions presented above, SAPO reactions occur under acidic conditions and this may offer alternative guest/host interactions. The gel compositions

used were: 1.0 Al<sub>2</sub>O<sub>3</sub>:1.0 P<sub>2</sub>O<sub>5</sub>:0.2 SiO<sub>2</sub>:0.3 SDA<sup>+</sup>OH<sup>-</sup>:0.3 HX:55.0 H<sub>2</sub>O, where X was Cl or F (HCl or HF). SAPO products reflect aluminophosphate (AlPO) frameworks and therefore contain even numbered rings exclusively<sup>48</sup>. Therefore, Beta would not be possible in these reactions as all polymorphs contain 5 MRs. Table 3.8 gives the phases obtained from SAPO reactions using **17** and **19**. Only AlPO<sub>4</sub>-5 (AFI) and an unknown dense phase were observed. AFI has a one-dimensional large pore structure and is commonly observed in AlPO reactions. The organic stabilizes the growing crystal in an analogous manner to high silica zeolite reactions. This indicates both **17** and **19** reside in the straight pores of AFI. The straight pores in Beta polymorphs A and B are approximately the same diameter as in AFI and this suggests both SDAs may reside in these channels rather than the desired [001] sinusoidal channel of polymorph A. As a default phase was obtained in the initial SAPO reactions additional experiments were not performed as AFI was expected to dominate.

Table 3.8: Phases obtained from silicoaluminophosphate (SAPO) inorganic reactions using **17** and **19**

SDA	SDA <sup>+</sup> OH <sup>-</sup> + HCl	SDA <sup>+</sup> OH <sup>-</sup> + HF
<b>18</b>	AFI <sup>a</sup>	AFI
<b>20</b>	Dense	AFI <sup>a</sup>

<sup>a</sup>Minor impurity present

The experimental results discussed above show two SDAs capable of synthesizing Beta but no detectable enrichment in polymorph A was observed. To gain further insight



into why no enrichment occurred molecular modeling was performed. Molecular modeling gives an estimated thermodynamic fit for a given guest/host pair plus a visual representation of possible organic conformations within the host. The modeling investigated guest/host interactions of **17** in \*BEA (P4<sub>1</sub>22) and EUO, and **19** in \*BEA (P4<sub>1</sub>22). No additional phases were considered for **19** as the experimental results presented above showed this SDA only synthesized Beta in high silica reactions.

SDA **17** was investigated first as two product phases were obtained allowing a comparison of the respective stabilization energies. The EUO pores consist of 10MR channels with deep side pockets delimited by 12MR openings. The SDA was found to nicely occupy the side pockets with calculated stabilization of  $-7.0 \text{ kJ mol}^{-1} \text{ T}_d \text{ atom}$ . The SDA size and location agrees with those found through single crystal diffraction techniques for dibenzyltrimethylammonium derived SDAs in ZSM-50 (EUO)<sup>49</sup>.

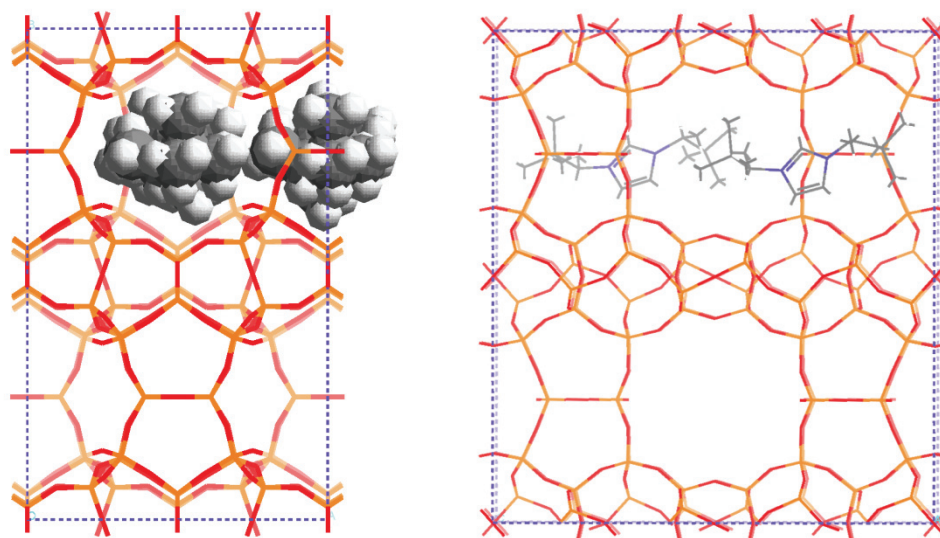


Figure 3.9: Energy-minimized location of **17** in EUO. Left panel shows [001] view perpendicular to [100] 10MR pore, right panel shows [100] view along 10MR pore

In contrast to EUO, \*BEA contains intersecting 12MR pores in all three crystallographic directions and several packing arrangements could be envisioned. Initial organic positions were investigated with molecules occupying the [100]/[010] pores exclusively as shown in Figure 3.10. The SDA molecules were accommodated in the straight pores with calculated stabilization of  $-10.2 \text{ kJ mol}^{-1} \text{ T}_d \text{ atom}$ . The stabilization energy was lower than reported for **VI** in each Beta polymorph ( $-11$  to  $-12 \text{ kJ mol}^{-1} \text{ T}_d \text{ atom}$ ). The slightly higher stabilization offered by the pyrrolidinium SDA **VI** could explain why greater ordering was observed compared to the present case. The calculated stabilization energies suggest more favorable interactions in \*BEA yet EUO was observed under several conditions underscoring the importance of kinetic factors. In addition to the calculated stabilization energy, the organic content was checked. The cell shown in Figure

3.10 contains 8 SDA molecules and 128 Si atoms. This corresponds to 19.8 wt% organic content as a fraction of the total cell mass. This agrees with the TGA data given in Table 3.4. In this configuration the SDA molecule does not project any “handedness” across the fault planes along [001]. To accommodate one SDA along [001] an adjacent SDA running perpendicular was impeded. To avoid overlap the adjacent SDA must be removed; however, this would lower the organic content and not agree with the observed TGA data.

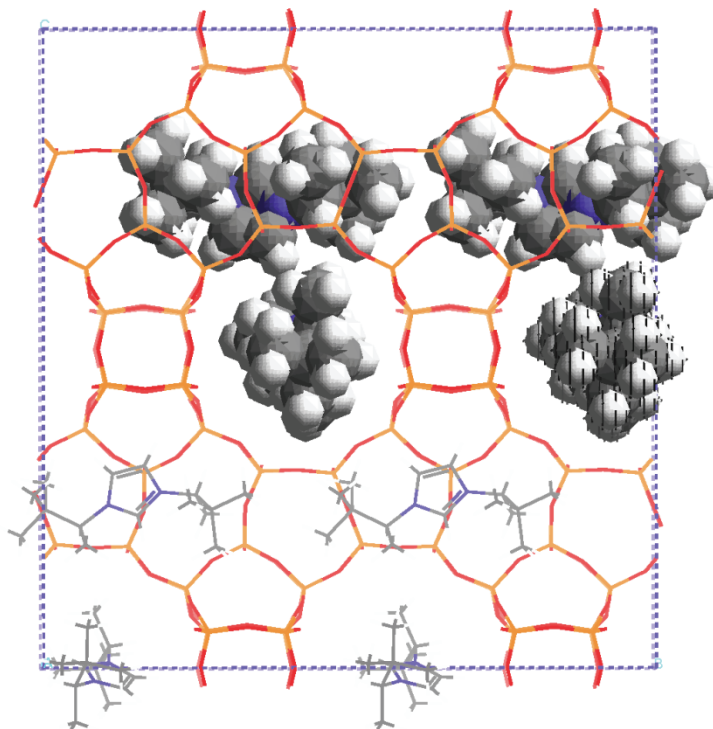


Figure 3.10: Energy-minimized location of **17** in \*BEA

For **19** in \*BEA a similar initial arrangement of [100]/[010] placement was implemented. In this case the larger SDA could be accommodated within the 12MR but with only one in each direction (the simulation cell was deeper compared to above). Figure

3.11 shows an energy minimized configuration for this case. This configuration did not fill the entire void volume efficiently with attempts to enlarge the cell further resulting in very slow energy minimizations. The cell as shown contains 8 SDA molecules and 256 Si atoms corresponding to 13.1 wt% organic content as a fraction of the total cell mass. Stabilization calculations gave  $-5.5 \text{ kJ mol}^{-1} \text{ T}_d \text{ atom}$ . While both are lower than reported for **17** the SDA does appear to fit within the straight 12MR pores again explaining why minimal ordering was observed. Rotating one SDA to align with the  $[001]$  pore gave overlap as described above.

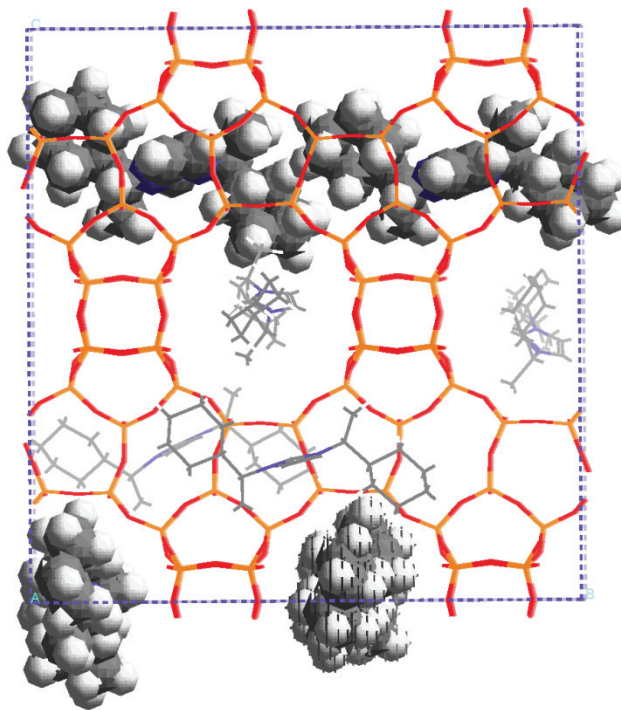


Figure 3.11: Energy minimized location of **19** in \*BEA

These simulations show careful consideration must be given to filling the entire available void volume while still trying to project chirality across the [001] fault planes. In this regard large SDA molecules have the length necessary to span a fault plane; however, efficiently filling the void volume becomes unlikely.

### 3.4: Conclusions

Guest/host relationships were investigated for a series of five chiral imidazolium SDAs aimed at synthesizing Beta polymorph A or another chiral product. 1,3-bis((S)-3,3-dimethylbutan-2-yl)imidazolium synthesized Beta and EUO, while 1,3-bis((S)-1-cyclohexylethyl)imidazolium only made Beta. XRD patterns for many products using both SDAs showed distinct differences by XRD to regular Beta, although this did not correspond to polymorph A enrichment. Molecular modeling combined with TGA indicated both molecules occupy the straight 12MR [100] and [010] pores of Beta polymorphs A and B. In this conformation no significant chirality was projected across the [001] fault planes explaining why no enrichment was observed. The remaining three SDAs did not direct the formation of any crystalline phases. Increased hydrophobicity for 1,3-bis((S)-1-cyclohexylpropyl)imidazolium and 1,3-bis(cis-Myrtanyl)imidazolium was likely responsible for not obtaining crystalline products. No similar argument could be made for 1,3-bis((S)-1-phenylethyl)imidazolium as it has the same  $\Sigma(C+N)$  as 1,3-bis((S)-1-cyclohexylethyl)imidazolium that successfully made Beta.

### 3.5: References

1. R. L. Wadlinger, G. T. Kerr and E. J. Rosinski, US Patent No. 3,308,069 (1967).
2. J. M. Newsam, M. M. J. Treacy, W. T. Koetsier and C. B. Degruyter, Proceedings of the Royal Society of London Series A—Mathematical Physical and Engineering Sciences **420** (1859), 375–405 (1988).
3. M. M. J. Treacy and J. M. Newsam, Nature **332** (6161), 249–251 (1988).
4. J. B. Higgins, R. B. Lapierre, J. L. Schlenker, A. C. Rohrman, J. D. Wood, G. T. Kerr and W. J. Rohrbaugh, Zeolites **8** (6), 446–452 (1988).
5. <http://www.iza-structure.org/databases/>.
6. J. H. Yu and R. R. Xu, Journal of Materials Chemistry **18** (34), 4021–4030 (2008).
7. L. Tang, L. Shi, C. Bonneau, J. Sun, H. Yue, A. Ojuva, B.-L. Lee, M. Kritikos, R. G. Bell, Z. Bacsik, J. Mink and X. Zou, Nat Mater **7** (5), 381–385 (2008).
8. J. Sun, C. Bonneau, A. Cantin, A. Corma, M. J. Diaz-Cabanas, M. Moliner, D. Zhang, M. Li and X. Zou, Nature **458** (7242), 1154–1157 (2009).
9. T. Blasco, A. Corma, M. J. Diaz-Cabanas, F. Rey, J. Rius, G. Sastre and J. A. Vidal-Moya, Journal of the American Chemical Society **126** (41), 13414–13423 (2004).
10. T. Conradsson, M. S. Dadachov and X. D. Zou, Microporous and Mesoporous Materials **41** (1–3), 183–191 (2000).
11. A. Corma, M. T. Navarro, F. Rey, J. Rius and S. Valencia, Angewandte Chemie International Edition **40** (12), 2277–2280 (2001).

12. Á. Cantín, A. Corma, M. J. Díaz-Cabaña, J. L. Jordá, M. Moliner and F. Rey, *Angewandte Chemie International Edition* **45** (47), 8013–8015 (2006).
13. M. Moliner, P. Serna, A. Cantin, G. Sastre, M. J. Diaz-Cabanas and A. Corma, *The Journal of Physical Chemistry C* **112** (49), 19547–19554 (2008).
14. A. W. Burton, S. Elomari, I. Chan, A. Pradhan and C. Kibby, *The Journal of Physical Chemistry B* **109** (43), 20266–20275 (2005).
15. M. M. J. Treacy, J. M. Newsam and M. W. Deem, *Proceedings of the Royal Society of London: Mathematical and Physical Sciences* **433** (1889), 499–520 (1991).
16. M. E. Davis and R. F. Lobo, *Chem. Mater.* **4** (4), 756–768 (1992).
17. W. A. Herrmann, L. J. Goossen, G. R. J. Artus and C. Kocher, *Organometallics* **16** (11), 2472–2477 (1997).
18. A. Alexakis, Caroline L. Winn, F. Guillen, J. Pytkowicz, S. Roland and P. Mangeney, *Advanced Synthesis & Catalysis* **345** (3), 345–348 (2003).
19. C. L. Winn, F. Guillen, J. Pytkowicz, S. Roland, P. Mangeney and A. Alexakis, *Journal of Organometallic Chemistry* **690** (24–25), 5672–5695 (2005).
20. M. C. Perry and K. Burgess, *Tetrahedron—Asymmetry* **14** (8), 951–961 (2003).
21. Y. Suzuki, K. Muramatsu, K. Yamauchi, Y. Morie and M. Sato, *Tetrahedron* **62** (2–3), 302–310 (2006).
22. T. Kano, K. Sasaki and K. Maruoka, *Organic Letters* **7** (7), 1347–1349 (2005).
23. Y. Kubota, M. M. Helmkamp, S. I. Zones and M. E. Davis, *Microporous Materials* **6** (4), 213–229 (1996).

24. K. Tsuji, P. Wagner and M. E. Davis, *Microporous and Mesoporous Materials* **28** (3), 461–469 (1999).
25. I. Ogino and M. E. Davis, *Microporous and Mesoporous Materials* **67** (1), 67–78 (2004).
26. R. F. Lobo and M. E. Davis, *Journal of the American Chemical Society* **117** (13), 3764–3779 (1995).
27. Y. Nakagawa, US Patent No. 5,271,922 (1993).
28. M. Yoshikawa, P. Wagner, M. Lovallo, K. Tsuji, T. Takewaki, C. Y. Chen, L. W. Beck, C. Jones, M. Tsapatsis, S. I. Zones and M. E. Davis, *Journal of Physical Chemistry B* **102** (37), 7139–7147 (1998).
29. A. Corma, M. J. Diaz-Cabanas, J. Martinez-Triguero, F. Rey and J. Rius, *Nature* **418** (6897), 514–517 (2002).
30. A. Corma, M. J. Diaz-Cabanas, M. Moliner and C. Martinez, *Journal of Catalysis* **241** (2), 312–318 (2006).
31. K. Tsuji and M. E. Davis, *Microporous Materials* **11** (1–2), 53–64 (1997).
32. A. Corma, M. Moliner, A. Cantin, M. J. Diaz-Cabanas, J. L. Lorda, D. L. Zhang, J. L. Sun, K. Jansson, S. Hovmoller and X. D. Zou, *Chemistry of Materials* **20** (9), 3218–3223 (2008).
33. M. D. Kadgaonkar, M. W. Kasture, D. S. Bhange, P. N. Joshi, V. Ramaswamy, N. M. Gupta and R. Kumar, *Microporous and Mesoporous Materials* **105** (1–2), 82–88 (2007).
34. M. D. Kadgaonkar, M. W. Kasture, D. S. Bhange, P. N. Joshi, V. Ramaswamy and R. Kumar, *Microporous and Mesoporous Materials* **101** (1–2), 108–114 (2007).



35. Y. Takagi, T. Komatsu and Y. Kitabata, *Microporous and Mesoporous Materials* **109** (1–3), 567–576 (2008).
36. M. Strotmann and H. Butenschon, *Synthetic Communications* **30** (22), 4173–4176 (2000).
37. W. J. McGahren and M. P. Kunstmann, *The Journal of Organic Chemistry* **37** (6), 902–906 (1972).
38. E. D. Burchart, V. A. Verheij, H. Vanbakkum and B. Vandegraaf, *Zeolites* **12** (2), 183–189 (1992).
39. A. K. Rappe, C. J. Casewit, K. S. Colwell, W. A. Goddard and W. M. Skiff, *Journal of the American Chemical Society* **114** (25), 10024–10035 (1992).
40. A. W. Burton, *Journal of the American Chemical Society* **129** (24), 7627–7637 (2007).
41. M. A. Camblor, P. A. Barrett, M.-J. Díaz-Cabañas, L. A. Villaescusa, M. Puche, T. Boix, E. Pérez and H. Koller, *Microporous and Mesoporous Materials* **48** (1–3), 11–22 (2001).
42. S. I. Zones, S. J. Hwang and M. E. Davis, *Chemistry—a European Journal* **7** (9), 1990–2001 (2001).
43. M. E. Davis and C. Saldarriaga, *Journal of the Chemical Society—Chemical Communications* (14), 920–921 (1988).
44. S. I. Zones, Y. Nakagawa, G. S. Lee, C. Y. Chen and L. T. Yuen, *Microporous and Mesoporous Materials* **21** (4–6), 199–211 (1998).
45. D. J. Earl, A. W. Burton, T. Rea, K. Ong, M. W. Deem, S.-J. Hwang and S. I. Zones, *J. Phys. Chem. C* **112** (24), 9099–9105 (2008).

46. Y. Chu, H. Deng and J. P. Cheng, *Journal of Organic Chemistry* **72** (20), 7790–7793 (2007).
47. T. L. Amyes, S. T. Diver, J. P. Richard, F. M. Rivas and K. Toth, *Journal of the American Chemical Society* **126** (13), 4366–4374 (2004).
48. A. W. Burton, *Zeitschrift Fur Kristallographie* **219** (12), 866–880 (2004).
49. M. Arranz, J. Perez-Pariente, P. A. Wright, A. M. Z. Slawin, T. Blasco, L. Gomez-Hortiguela and F. Cora, *Chem. Mater.* **17** (17), 4374–4385 (2005).